Single-qubit anisotropy induced by micromagnet in Si-MOS quantum dot

Ning, Kai Chun; Zhang, X.; Ma, Rong-Long ; Kong, Zhen-Zhen ; Liao, Wei-Zhu ; Zhu, Sheng-Kai ; Wang, Chu ; Wang, Gui-Lei ; Li, Hai-Ou ; More Authors

DOI
10.35848/1882-0786/adaad7

Publication date
2025

Document Version
Final published version

Published in
Applied Physics Express

Applied Physics
Express

Single-qubit anisotropy induced by micromagnet in Si-MOS quantum dot

OPEN ACCESS
Applied Physics Express 18, 012006 (2025) LETTER
https://doi.org/10.35848/1882-0786/adaad7

Check for updates

Single-qubit anisotropy induced by micromagnet in Si-MOS quantum dot

Ning Chu[1,2], Xin Zhang[3], Rong-Long Ma[1,2], Zhen-Zhen Kong[4], Wei-Zhu Liao[1,2], Sheng-Kai Zhu[1,2], Chu Wang[1,2], Ao-Ran Li[1,2], Gui-Lei Wang[5,6], Gang Cao[1,2,5], Hai-Ou Li[1,2,5*], and Guo-Ping Guo[1,2,5,7]

[1]*CAS Key Laboratory of Quantum Information, University of Science and Technology of China, Hefei, Anhui 230026, People's Republic of China*
[2]*CAS Center for Excellence in Quantum Information and Quantum Physics, University of Science and Technology of China, Hefei, Anhui 230026, People's Republic of China*
[3]*QuTech and Kavli Institute of Nanoscience, Delft University of Technology, Lorentzweg 1, 2628 CJ Delft, The Netherlands*
[4]*Integrated Circuit Advanced Process R&D Center, Institute of Microelectronics, Chinese Academy of Sciences, Beijing 100029, People's Republic of China*
[5]*Hefei National Laboratory, University of Science and Technology of China, Hefei 230088, People's Republic of China*
[6]*Beijing Superstring Academy of Memory Technology, Beijing 100176, People's Republic of China*
[7]*Origin Quantum Computing Company Limited, Hefei, Anhui 230088, People's Republic of China*

*E-mail: haiouli@ustc.edu.cn

Received December 5, 2024; revised December 25, 2024; accepted January 15, 2025; published online January 28, 2025

Synthesized spin–orbit coupling (SSOC) is crucial for the operation of spin qubits in silicon quantum dot, as it address the challenge posed by the inherently weak intrinsic spin–orbit coupling in silicon. Here, we investigate the anisotropic properties of single spin qubit in silicon metal-oxide-semiconductor (Si-MOS) quantum dot and provide experimental evidence for the control of SSOC. Additionally, we experimentally demonstrate that tuning the operating point away from the conventional configuration can enhance the quality factor of the spin qubit. These findings lay a foundation for the realization of high-quality tunable spin–orbit qubits.

Supplementary material for this article is available online

Among the various quantum computing systems, electron spins in semiconductor quantum dots provides an attractive platform for quantum information processing.[1–5] Coherent control of electron spins can be achieved through electron spin resonance by applying an alternating magnetic field.[6] Alternatively, another commonly employed method for controlling electron spins in silicon-based systems involves the integration of a micromagnet to provide a stray gradient field, which is a synthetic spin–orbit coupling (SSOC), allowing for electrical manipulation known as electric-dipole spin resonance.[7,8] Recently, significant advancements have been achieved in implementing quantum error correction protocols, as demonstrated by single-qubit gates with fidelities exceeding 99.9%[9,10] and two-qubit gates achieving fidelities as high as 99%.[11–14]

Different from the intrinsic spin–orbit coupling (ISOC) arising from the underlying material or structural asymmetries, SSOC is introduced by the magnetic field gradient of integrated micromagnet, which breaks time-reversal symmetry.[15,16] However, the presence of micromagnet near the quantum dots can also expose the qubits to electric noise, leading to a rapid relaxation and decoherence of the spin qubit.[9,17–21] The different shapes of micromagnet and their varying relative positions to quantum dots can cause the qubits to experience different stray gradient fields in various directions. For ISOC, previous studies have demonstrated the impact of changing the magnetic field direction on qubit properties,[22–29] primarily by altering the anisotropy of the Dresselhaus term in the spin–orbit coupling to partially counteract the effects of the Rashba term. In comparison, the effect of SSOC in different magnetic field direction on the qubit properties, like qubit dephasing times (T_2^*, T_2^{rabi}), Rabi frequencies (f_{rabi}) and the quality factor (such as Q^{rabi}), is yet to be investigated.[30]

Here, we study the effects of SSOC fields generated by bar micromagnet on the single-spin qubit properties. First, we measured the Larmor frequency of a single qubit with different magnetic field angles, revealing a sinusoidal trend as a function of the external magnetic field angle. Second, we measured the anisotropic of Rabi frequency, which shows a significant non-sinusoidal modulation, in contrast to the Larmor frequency.[30] Finally, we compared f_{rabi} to T_2^{rabi} and calculated $Q^{\mathrm{rabi}} = 2f_{\mathrm{rabi}}T_2^{\mathrm{rabi}}$, which shows the quality factor of the spin qubit is enhanced by tuning the magnetic field angle away from the conventional configuration.

We fabricated a highly tunable Si-MOS double quantum dot device incorporating multi-level aluminum gate-stacks on an isotopically enriched ^{28}Si substrate, with a residual concentration of ^{29}Si at 60 ppm.[31,32] The device is located in a dilution refrigerator operating at a base temperature of approximately 20 mK and its layout is illustrated in Fig. 1(a). Gates C1 and C2 provide a pathway for electrons to flow between the reservoirs under gate S1 and gate S5. A single-electron transistor (SET) is located beneath gate S3, while gates S2 and S4 define the barriers of the SET. Gates C2 and C3 define the lateral channel for electron tunneling, and the reservoir (in orange) under gate RG supplies electrons to the quantum dots. The quantum dots are formed under gates LP and RP, with the gate MB designed to tune the tunnel coupling between two quantum dots. The yellow bar in the Fig. 1(a) represents a rectangular Ti/Co micromagnet, with its length oriented along the y-axis, width along the x-axis, and a thickness of 10/250 nm (detailed structural parameters can be found in Supplementary Note 2). The applied in-plane magnetic field B_{ext} is directed with an angle θ_{B} relative to the x-axis ([110]). The right inset shows the stray fields to generate SSOC, with components $\boldsymbol{B}_{//}$ parallel to $\boldsymbol{B}_{\mathrm{ext}}$, $\boldsymbol{B}_{\perp}$ perpendicular to $\boldsymbol{B}_{\mathrm{ext}}$ in the x–y plane, and $\boldsymbol{B}_z$ perpendicular to both $\boldsymbol{B}_{\mathrm{ext}}$ and the x–y plane. Figure 1(b) presents the charge stability diagram (Q_{L}, Q_{R}) for two quantum dots with charge

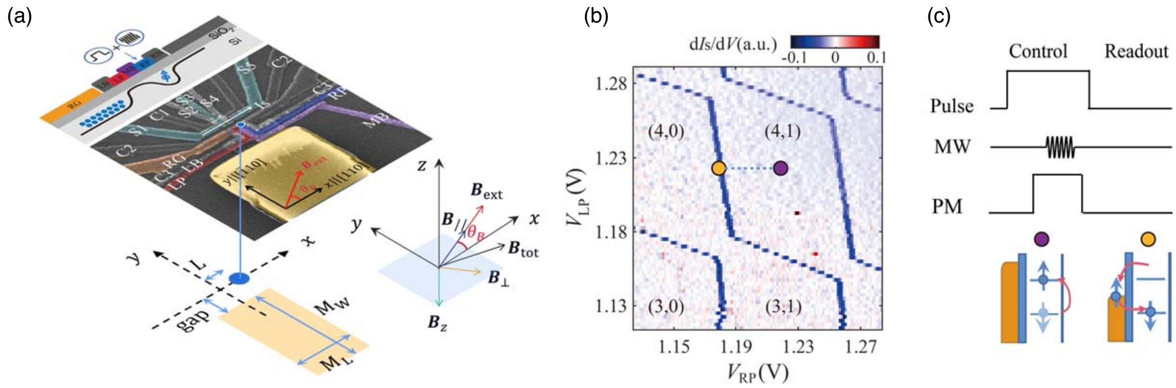

Fig. 1. (a) A schematic diagram and a false-color scanning electron microscope image corresponding to the device measured in the experiment. The gate electrodes and micromagnet are indicated. The current *Is* through the SET is represented by a white arrow. The angle between the external magnetic field $\boldsymbol{B}_{ext}$ and the *x*-axis is θ_B. Below the SEM image is a schematic diagram illustrating the geometric relationship between the micromagnet and the Q_R quantum dot, where geometric modeling of the micromagnet structure was performed. Inset: cartesian coordinates and labels for different magnetic fields. (b) The charge stability diagram of the two quantum dots formed beneath LP and RP is presented. The number of electrons in these dots is denoted as (Q_L, Q_R). The orange circles indicate the readout positions, while the purple circles represent the control positions. (c) A schematic diagram of the measurement scheme, illustrating how a DC voltage, along with pulse and microwave (MW) waveforms, is applied to the RP electrode through a bias-tee. During the control phase (10 ms), the qubit is driven by microwave bursts, with pulse modulation (PM) facilitating the control of the microwave switch, allowing for a higher microwave switching ratio. In the readout phase (10 ms), energy-selective readout is performed. If the electron is in spin-up state, it can tunnel into the electron reservoir and load a spin- down electron, thus completing the initialization process. Conversely, if the electron is in a down-spin state, no transition occurs.

occupancy. The charge occupancy is detected by measuring the differential SET current *dIs*/*dV*. The electrons in the left quantum dot (Q_L) completely fill the first shell ($v_- \downarrow$, $v_- \uparrow$, $v_+ \downarrow$, $v_+ \uparrow$),[33] where $v_-(v_+)$ represents the ground state (excited state) energy level of the valley, thereby minimizing the impact on the electron transition in the right quantum dot. The electrons in the quantum dot on the right are at the energy level of the ground state valley, because we found through magnetospectroscopy measurement that there is no crossing point of spin-valley coupling when the external magnetic field exceeds 2 T. This shows that the valley splitting in our Si-MOS sample is large enough, and the v_+ energy level of the right dot is not considered within the magnetic field range of our experiment. The complete measurement scheme is illustrated in Fig. 1(c), which involves applying resonant microwaves during the control phase to flip electrons initialized in the spin-down state to the spin-up state. During the readout phase, energy-selective measurements are performed.[31,34–36]

Figure 2(a) presents the results of the spin fraction under the application of a chirp pulse[36] at an external magnetic field $B_{ext}(\theta_B = 0°) = 777$ mT. We use frequency chirped microwave bursts, and when the excitation frequency passes through the resonance frequency, the electron spin is inverted. As shown in Fig. 2(b), by rotating the external magnetic field $\boldsymbol{B}_{ext}$ with an angle θ_B relative to the *x*-axis while keeping the microwave frequency constant at 24.5 GHz, we scanned the external magnetic field strength and found that the resonant magnetic field was sinusoidally modulated, with a period of 180° and a phase shift of 8.3°. The Larmor frequency f_L can be calculated by $hf_L = g\mu_B \boldsymbol{B}_{tot}$, where h is Planck constant, μ_B is the Bohr magneton, g-factor is typically around 2 in silicon, and $\boldsymbol{B}_{tot} = \boldsymbol{B}_{ext} + \boldsymbol{B}_{//} + \boldsymbol{B}_\perp + \boldsymbol{B}_z$ determines the electron quantization axis. To compare with the experimental results, we numerically calculated the stray field generated by the micromagnet in different directions. As shown in Fig. 2(b), the component $\boldsymbol{B}_{//}$ (deep blue curve), which is parallel to $\boldsymbol{B}_{ext}$, shows an almost out-of-phase modulation relative to the resonance peaks. This negative correlation can be understood by the fact that the external magnetic field $\boldsymbol{B}_{ext}$ dominates the total magnetic field, meaning that the direction of the total field is nearly aligned with $\boldsymbol{B}_{ext}$. Furthermore, the orange and green curves represent the calculated values of $\boldsymbol{B}_\perp$ and $\boldsymbol{B}_z$, respectively, as a function of θ_B. The former has a period of 180°, like $\boldsymbol{B}_{//}$, while the latter has a period of 360°. For the detailed calculation procedure, please refer to Supplementary Note 2.

We then measured Rabi oscillations at different magnetic directions. Two traces from the measurements are shown in Fig. 3(a), at directions of $\theta_B = 90°$ and 340°, showing a clear anisotropy. We extract f_{rabi} and T_2^{rabi} by fitting the rabi oscillation. The fitting formula is $P_\uparrow = A \times \exp(-t_{MW}/T_2^{rabi}) \sin(2\pi f_{rabi} + \varphi) + B$, where A is a scaling factor, B is an offset and the phase factor φ is a fitting parameter. In contrast to the sinusoidal modulation trend observed with respect to the angle of the external magnetic field $\boldsymbol{B}_{ext}$, f_{rabi} presents a non-sinusoidal modulation under the condition of equal microwave frequency [Fig. 3(b)]. The non-sinusoidal behavior diverges from the anisotropic sinusoidal trend induced by ISOC[25] and is attributed to SSOC generated by the micromagnet. We performed micromagnet simulations and calculate the total transverse magnetic field gradient as $b_{tr} = d\boldsymbol{B}_{tr}^{tot}/dy$, considering the electron displacement direction is along the y axis. We then calculated the Rabi frequency $f_{rabi}^{sim} \sim C \cdot b_{tr}$, where C is a scaling factor (see Supplementary Note 4), which reproduced the fundamental characteristics of the experimental results.[25,37] The discrepancy between the experimental and calculated minimum Rabi frequency may be attributed to the presence of ISOC in the silicon material. The non-sinusoidal behavior of the resonance amplitude is a direct consequence of the competing contributions of the

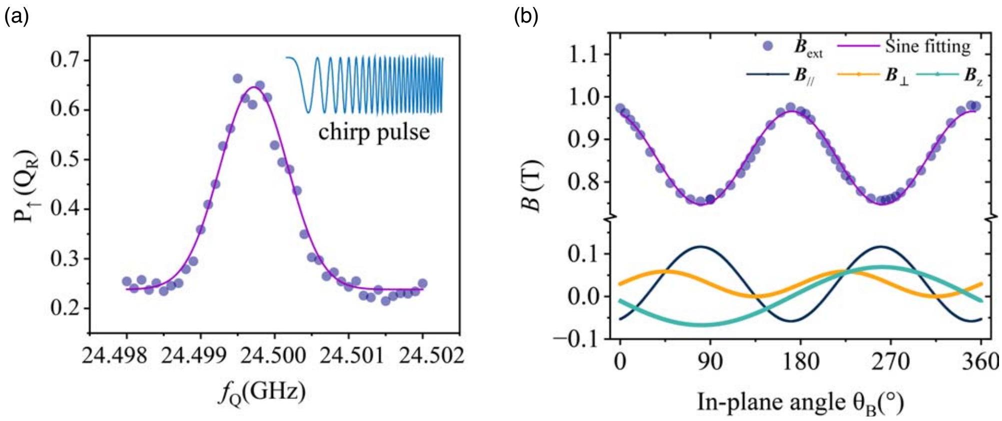

Fig. 2. (a) A 1 MHz chirped pulse of microwave excitation of 500 μs with variable frequency adiabatically flip one the spin into a spin-up configuration. The spin fraction as a function of the microwave frequency of an applied chirp pulse, with the electron state initialized to spin-down, reveals that the resonant frequency of Q_R is 24.4998 GHz. The data is fitted using a Gaussian peak function. (b) The measured resonant magnetic field strengths (purple circles) as a function of the in-plane magnetic field angle θ_B with a fixed microwave frequency of 24.5 GHz. A cosine fit of the data with the equation $A\cos(2\pi\theta_B + \phi) + B$ is applied, where A is a scaling factor, B is an offset and the phase factor $\phi = 8.3°$ may arise from the asymmetry of the quantum dot and the bar magnet in the spatial y-direction. The components $\boldsymbol{B}_{//}$, $\boldsymbol{B}_{\perp}$, and $\boldsymbol{B}_z$ are obtained by calculating the magnetic field strengths corresponding to different magnetization directions of the micromagnet.

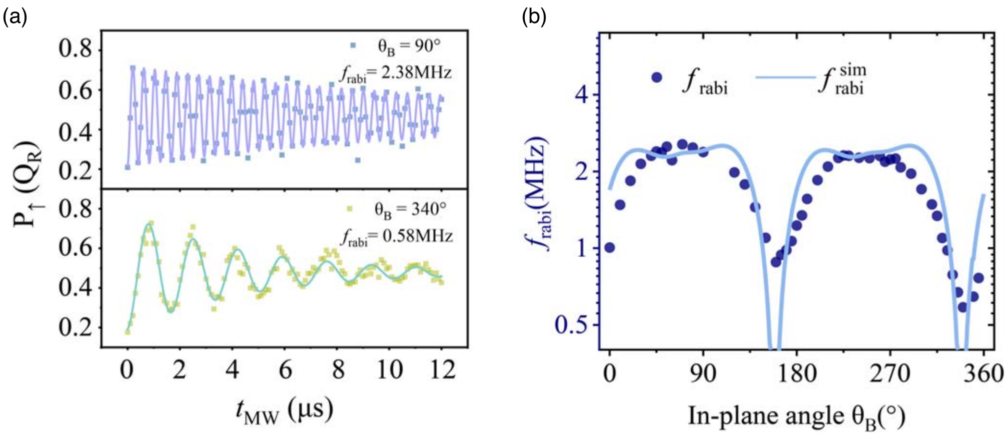

Fig. 3. (a) Upper part: Rabi oscillations at $\theta_B = 90°$ (where the external magnetic field is directed along the y-axis), with a Rabi frequency of $f_{rabi} = 2.38(3)$ MHz. Lower part: Rabi oscillations at $\theta_B = 340°$, with $f_{rabi} = 0.58(6)$ MHz. The maximum and minimum values of the Rabi frequency differ by approximately a factor of 4.1. (b) The measured (dark blue circles) and calculated (light blue line) Rabi frequency f_{rabi} as a function of the in-plane magnetic field angle θ_B. The microwave frequency and power are kept constant throughout the experiment.

out-of-plane and in-plane transverse magnetic field gradients to the SSOC (Supplementary Note 3).

The micromagnet not only provides a transverse gradient field that can be used for driving but also generates a longitudinal gradient field that causes decoherence. The primary components contributing to this decoherence are $d\boldsymbol{B}_{long}/dy$ and $d\boldsymbol{B}_{long}/dx$, which, along with charge noise, are likely the most significant sources of decoherence in our device. We also conducted tests of Q^{rabi} at different angles θ_B. Similar to the results for f_{rabi}, Q^{rabi} also exhibits an anisotropic trend with a clear non-sinusoidal characteristic, where $Q^{rabi}_{max} \sim 100$ at $\theta_B = 270°$ and $Q^{rabi}_{min} \sim 5$ at $\theta_B = 340°$ as shown in Fig. 4. The optimal quality factor location is not along the y-axis but at a certain angle deviating from it, and our calculations of the gradient magnetic field also confirms that. Considering that the transverse gradient and the longitudinal gradient are responsible for Rabi oscillations and decoherence, respectively, and assuming that charge noise is isotropic, we defined the quality factor $Q = (d\boldsymbol{B}^{tot}_{tr}/dy)/\sqrt{(d\boldsymbol{B}_{long}/dy)^2 + (d\boldsymbol{B}_{long}/dx)^2}$ (Supplementary

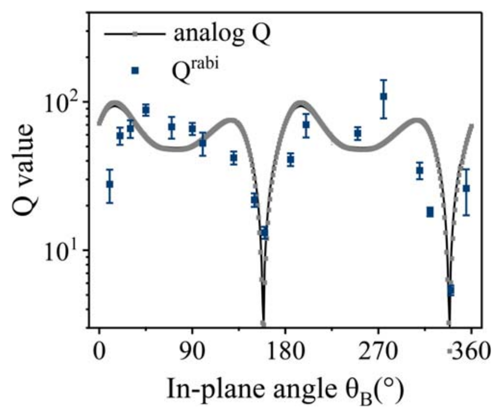

Fig. 4. The relationship between the quality factor and the angle of the external magnetic field. The gray curve represents the magnetic field gradient obtained from numerical simulations and the calculated quality factor Q as a function of the external magnetic field direction θ_B. The optimal angle for the quality factor deviates from the y-axis by a certain angle. The maximum Q factors obtained from numerical calculations are located at angles of 15° and 130°. For detailed computation processes, see Supplementary Note 3.

Note 3). At certain angles deviating from the *y*-axis (15° and 130°), the longitudinal gradient $d\boldsymbol{B}_{\mathrm{long}}/dy$ is significantly suppressed, while the transverse gradient $d\boldsymbol{B}_{\mathrm{tr}}^{\mathrm{tot}}/dy$ remains relatively high, thereby optimizing the quality factor of the qubit. In addition, the calculated $d\boldsymbol{B}_{\mathrm{long}}/dx$ can also be utilized for the spin addressability of our device, indicating that it is enhanced at the angle where the quality factor is maximized.

This study investigates the anisotropic behavior of the Larmor frequency f_{L}, the Rabi frequency f_{rabi} and the decoherence time under qubit driving T_2^{rabi} induced by stray gradient fields from micromagnet, which distinguishes SSOC from ISOC. We predict that if the direction of the in-plane magnetic field deviates from the conventional operating point, the quality factor of the spin qubit can be optimized while minimizing the effects of charge noise, thus maintaining effective electric dipole spin control.

Compared with ISOC, which could be strongly influenced by microscopic features of the interface that are difficult to control, SSOC is mainly dependent on the micromagnet design whose properties can be reliably predicted by numerical calculations. Additionally, the structure of the micromagnet and its position relative to the quantum dot can be optimized based on numerical simulations to enhance the quality factor and drive strength of the single qubit. Although the magnetization direction of the micromagnet is determined after deposition, further optimization can still be achieved by varying the angle of the rotating magnetic field. For future studies, the anisotropic of behavior of SSOC can also be investigated for spin shuttling or hopping spin qubits.[38–40]

Acknowledgments This work was supported by the National Natural Science Foundation of China (Grant Nos. 12474490, 92165207, 12034018 and 92265113), the Innovation Program for Quantum Science and Technology (Grant No. 2021ZD0302300), the USTC Tang Scholarship. This work was partially carried out at the USTC Center for Micro and Nanoscale Research and Fabrication.

1) R. Hanson, L. P. Kouwenhoven, J. R. Petta, S. Tarucha, and L. M. K. Vandersypen, Rev. Mod. Phys. **79**, 1217 (2007).
2) F. A. Zwanenburg, A. S. Dzurak, A. Morello, M. Y. Simmons, L. C. L. Hollenberg, G. Klimeck, S. Rogge, S. N. Coppersmith, and M. A. Eriksson, Rev. Mod. Phys. **85**, 961 (2013).
3) G. Burkard, T. D. Ladd, A. Pan, J. M. Nichol, and J. R. Petta, Rev. Mod. Phys. **95**, 025003 (2023).
4) X. Zhang, H. O. Li, G. Cao, M. Xiao, G. C. Guo, and G. P. Guo, Natl Sci. Rev. **6**, 32 (2019).
5) X. Zhang, H. O. Li, K. Wang, G. Cao, M. Xiao, and G. P. Guo, Chin. Phys. B **27**, 020305 (2018).
6) F. H. L. Koppens, C. Buizert, K. J. Tielrooij, I. T. Vink, K. C. Nowack, T. Meunier, L. P. Kouwenhoven, and L. M. K. Vandersypen, Nature **442**, 766 (2006).
7) K. C. Nowack, F. H. L. Koppens, Y. V. Nazarov, and L. M. K. Vandersypen, Science **318**, 1430 (2007).
8) M. Pioro-Ladrière, T. Obata, Y. Tokura, Y. S. Shin, T. Kubo, K. Yoshida, T. Taniyama, and S. Tarucha, Nat. Phys. **4**, 776 (2008).
9) J. Yoneda et al., Nat. Nanotechnol. **13**, 102 (2017).
10) C. H. Yang et al., Nat. Electron. **2**, 151 (2019).
11) M. T. Mądzik et al., Nature **601**, 348 (2022).
12) A. Noiri, K. Takeda, T. Nakajima, T. Kobayashi, A. Sammak, G. Scappucci, and S. Tarucha, Nature **601**, 338 (2022).
13) X. Xue, M. Russ, N. Samkharadze, B. Undseth, A. Sammak, G. Scappucci, and L. M. K. Vandersypen, Nature **601**, 343 (2022).
14) A. R. Mills, C. R. Guinn, M. J. Gullans, A. J. Sigillito, M. M. Feldman, E. Nielsen, and J. R. Petta, Sci. Adv. **8**, 5130 (2022).
15) P. Huang and X. Hu, npj Quantum Inf. **7**, 162 (2021).
16) P. H. Huang and X. D. Hu, New J. Phys. **24**, 013002 (2022).
17) A. Kha, R. Joynt, and D. Culcer, Appl. Phys. Lett. **107**, 172101 (2015).
18) E. Kawakami et al., Proc. Natl Acad. Sci. **113**, 11738 (2016).
19) F. Borjans, D. M. Zajac, T. M. Hazard, and J. R. Petta, Phys. Rev. Appl. **11**, 044063 (2019).
20) A. Hollmann et al., Phys. Rev. Appl. **13**, 034068 (2020).
21) T. Struck et al., npj Quantum Inf. **6**, 40 (2020).
22) P. Scarlino, E. Kawakami, P. Stano, M. Shafiei, C. Reichl, W. Wegscheider, and L. M. K. Vandersypen, Phys. Rev. Lett. **113**, 256802 (2014).
23) A. Hofmann, V. F. Maisi, T. Krähenmann, C. Reichl, W. Wegscheider, K. Ensslin, and T. Ihn, Phys. Rev. Lett. **119**, 176807 (2017).
24) L. C. Camenzind, L. Yu, P. Stano, J. D. Zimmerman, A. C. Gossard, D. Loss, and D. M. Zumbühl, Nat. Commun. **9**, 3454 (2018).
25) A. Corna et al., npj Quantum Inf. **4**, 6 (2018).
26) R. Ferdous et al., npj Quantum Inf. **4**, 26 (2018).
27) R. M. Jock et al., Nat. Commun. **9** (2018).
28) T. Tanttu et al., Phys. Rev. **9**, 021028 (2019).
29) X. Zhang et al., Phys. Rev. Lett. **124**, 257701 (2020).
30) X. Zhang et al., Phys. Rev. Appl. **15**, 044042 (2021).
31) R. L. Ma et al., Phys. Rev. Appl. **21**, 014044 (2024).
32) R. Z. Hu et al., Appl. Phys. Lett. **122**, 134002 (2023).
33) R. C. C. Leon et al., Nat. Commun. **11**, 797 (2020).
34) R. Hanson, L. H. W. van Beveren, I. T. Vink, J. M. Elzerman, W. J. M. Naber, F. H. L. Koppens, L. P. Kouwenhoven, and L. M. K. Vandersypen, Phys. Rev. Lett. **94**, 1 (2005).
35) A. Morello et al., Nature **467**, 687 (2010).
36) R. Z. Hu et al., Nanomaterials **11**, 2486 (2021).
37) T. Obata, M. Pioro-Ladrière, Y. Tokura, Y-S. Shin, T. Kubo, K. Yoshida, T. Taniyama, and S. Tarucha, Phys. Rev. B **81**, 085317 (2010).
38) C. A. Wang et al., Science **385**, 447 (2024).
39) M. De Smet et al., High-fidelity single-spin shuttling in silicon (2024), arXiv:2406.07267.
40) A. M. J. Zwerver, S. Amitonov, S. L. de Snoo, M. T. Madzik, M. Rimbach-Russ, A. Sammak, G. Scappucci, and L. M. K. Vandersypen, PRX Quantum **4**, 030303 (2023).